



# On $[H^1]^{3 \times 3}$ , $[H(\text{curl})]^3$ and $H(\text{sym Curl})$ finite elements for matrix-valued Curl problems

Adam Sky · Ingo Muench · Patrizio Neff

Received: 18 February 2022 / Accepted: 10 August 2022  
© The Author(s) 2022

**Abstract** In this work we test the numerical behaviour of matrix-valued fields approximated by finite element subspaces of  $[H^1]^{3 \times 3}$ ,  $[H(\text{curl})]^3$  and  $H(\text{sym Curl})$  for a linear abstract variational problem connected to the relaxed micromorphic model. The formulation of the corresponding finite elements is introduced, followed by numerical benchmarks and our conclusions. The relaxed micromorphic continuum model reduces the continuity assumptions of the classical micromorphic model by replacing the full gradient of the microdistortion in the free energy functional with the Curl. This results in a larger solution space for the microdistortion, namely  $[H(\text{curl})]^3$  in place of the classical  $[H^1]^{3 \times 3}$ . The continuity conditions on the microdistortion can be further weakened by taking only the symmetric part of the Curl. As shown in recent works, the new appropriate space for the microdistortion is then  $H(\text{sym Curl})$ . The newly introduced space gives rise to a new differential complex for the relaxed micromorphic continuum theory.

**Keywords** Approximation error · Finite elements · Nédélec elements · Relaxed micromorphic continuum · Relaxed micromorphic complex · sym Curl elements

## 1 Introduction

Today there exist various formulations of micromorphic continua [1–4] and higher gradient theories [5] with the common goal of capturing micro-motions that are unaccounted for in the classical Cauchy continuum theory. The unifying characteristic of all micromorphic theories is the extension of the mathematical model with additional degrees of freedom (called the microdistortion) for the material point. Consequently, in the general micromorphic theory, as introduced by Eringen [6] and Mindlin [7], each material point is endowed with nine extra degrees of

---

A. Sky (✉) · I. Muench  
Institute of Structural Mechanics, Statics and Dynamics, Technische Universität Dortmund, August-Schmidt-Str. 8, 44227  
Dortmund, Germany  
e-mail: adam.sky@tu-dortmund.de

I. Muench  
e-mail: ingo.muench@tu-dortmund.de

P. Neff  
Chair for Nonlinear Analysis and Modelling, Faculty of Mathematics, Universität Duisburg-Essen, Thea-Leymann Str. 9, 45127  
Essen, Germany  
e-mail: patrizio.neff@uni-due.de

freedom given by the matrix  $\mathbf{P}$ , capturing affine displacements that are independent of the translational degrees of freedom, such as rotation or expansion of the micro-body.

The relaxed micromorphic continuum [4, 8] differs from other micromorphic theories by reducing the continuity assumptions on these micro-motions. Instead of incorporating the full gradient  $D\mathbf{P}$  of the microdistortion into the free energy functional, the relaxed micromorphic continuum assumes only the Curl of the microdistortion to produce significant energies. As a result, the natural space for the microdistortion in the relaxed micromorphic continuum is  $[H(\text{curl})]^3$  (see also the related microcurl and gradient plasticity theories [9–12]). Further, the micro-dislocation, i.e.  $\text{Curl } \mathbf{P}$ , remains a second-order tensor, in contrast to the general micromorphic theory where the full gradient yields a third-order tensor  $D\mathbf{P} \in \mathbb{R}^{3 \times 3 \times 3}$ . Possible applications for the relaxed micromorphic theory, such as the simulation of metamaterials and bandgap materials, are demonstrated in [13, 14]. Further, closed-form solutions for specimen under shear, bending and torsion have already been derived in [15–17]. A first numerical implementation for a relaxed micromorphic model of antiplane shear can be found in [18], followed by an implementation for plain-strain models [19] and lastly, an implementation of the full three-dimensional model [20].

In recent works [21–26] it was shown that the continuity assumptions on the microdistortion can be weakened further by considering solely the symmetric micro-dislocation  $\text{sym Curl } \mathbf{P}$ . The corresponding space for the microdistortion is the Hilbert space  $H(\text{sym Curl})$ . A version of this space is also used for some formulations of the biharmonic equation [27], with a restriction to trace-free tensors.

In order to gain insight into the numerical behaviour of the microdistortion in these spaces and the potential meaning for the relaxed micromorphic continuum theory, we investigate three finite element formulations for  $\mathbf{P} \in [H^1]^{3 \times 3}$ ,  $\mathbf{P} \in [H(\text{curl})]^3$  and  $\mathbf{P} \in H(\text{sym Curl})$  on an abstract problem derived from the relaxed micromorphic continuum. We compare standard Lagrangian, Nédélec- [18, 28–31] and the recently introduced  $H(\text{sym Curl})$ -base functions [32], respectively.

This paper is organized as follows: In the first two sections we introduce the relaxed micromorphic continuum and derive a related abstract problem. Section 4 is devoted to the description of the finite element formulations. In Sect. 5 we present numerical examples and investigate their behaviour. The last section presents our conclusions and outlook.

## 2 A relaxed micromorphic complex

The relaxed micromorphic continuum [4, 8] is described by its free energy functional, incorporating the gradient of the displacement field, the microdistortion and its Curl

$$\begin{aligned}
 I(\mathbf{u}, \mathbf{P}) &= \frac{1}{2} \int_{\Omega} \langle \mathbb{C}_e \text{sym}(\mathbf{D}\mathbf{u} - \mathbf{P}), \text{sym}(\mathbf{D}\mathbf{u} - \mathbf{P}) \rangle + \langle \mathbb{C}_{\text{micro}} \text{sym } \mathbf{P}, \text{sym } \mathbf{P} \rangle \\
 &\quad + \langle \mathbb{C}_c \text{skew}(\mathbf{D}\mathbf{u} - \mathbf{P}), \text{skew}(\mathbf{D}\mathbf{u} - \mathbf{P}) \rangle + \mu_{\text{macro}} L_c^2 \|\text{Curl } \mathbf{P}\|^2 dX - \int_{\Omega} \langle \mathbf{u}, \mathbf{f} \rangle - \langle \mathbf{P}, \mathbf{M} \rangle dX, \\
 \mathbf{D}\mathbf{u} &= \begin{bmatrix} u_{1,1} & u_{1,2} & u_{1,3} \\ u_{2,1} & u_{2,2} & u_{2,3} \\ u_{3,1} & u_{3,2} & u_{3,3} \end{bmatrix}, \quad \text{Curl } \mathbf{P} = \begin{bmatrix} \text{curl} [P_{11} \ P_{12} \ P_{13}] \\ \text{curl} [P_{21} \ P_{22} \ P_{23}] \\ \text{curl} [P_{31} \ P_{32} \ P_{33}] \end{bmatrix}, \quad \text{curl } \mathbf{v} = \nabla \times \mathbf{v}, \tag{2.1}
 \end{aligned}$$

where  $\langle \cdot, \cdot \rangle$  denotes the scalar product on  $\mathbb{R}^{3 \times 3}$ ,  $\Omega \subset \mathbb{R}^3$  is the domain and  $\mathbf{u} : \Omega \subset \mathbb{R}^3 \rightarrow \mathbb{R}^3$  and  $\mathbf{P} : \Omega \subset \mathbb{R}^3 \rightarrow \mathbb{R}^{3 \times 3}$  represent the displacement and the non-symmetric microdistortion, respectively. The volume forces and micro-moments are given by  $\mathbf{f}$  and  $\mathbf{M}$ . Here,  $\mathbb{C}_e$  and  $\mathbb{C}_{\text{micro}}$  are standard fourth elasticity tensors and  $\mathbb{C}_c$  is a positive semi-definite coupling tensor for rotations. The macroscopic shear modulus is denoted by  $\mu_{\text{macro}}$  and the parameter  $L_c > 0$  represents the characteristic length scale motivated by the microstructure. The corresponding Hilbert spaces and their respective traces read

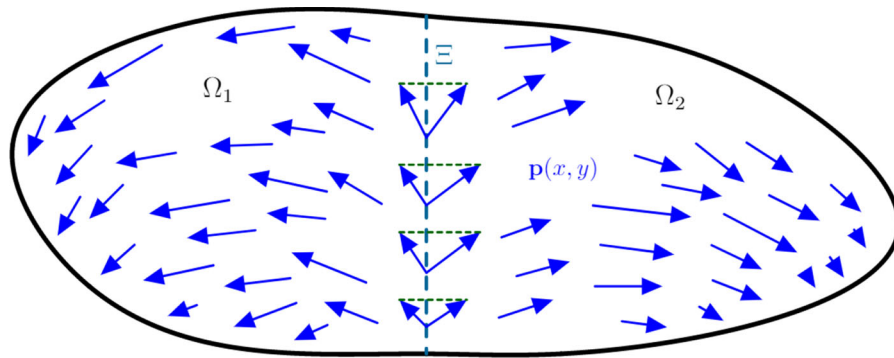


**Fig. 1** An example for a vector field  $\mathbf{p} \in H(\text{curl}, \Omega)$ . Note that  $\mathbf{p} \notin [H^1(\Omega)]^2$  since on the interface  $\Xi$ , only the tangential component of the vector field is continuous

$$H^1(\Omega) = \{u \in L^2(\Omega) \mid \nabla u \in [L^2(\Omega)]^3\}, \quad \text{tr}_{H^1} u = u \Big|_{\partial\Omega}, \tag{2.2}$$

$$H(\text{curl}, \Omega) = \{\mathbf{p} \in [L^2(\Omega)]^3 \mid \text{curl } \mathbf{p} \in [L^2(\Omega)]^3\}, \quad \text{tr}_{H(\text{curl})} \mathbf{p} = \mathbf{p} \times \boldsymbol{\nu} \Big|_{\partial\Omega}. \tag{2.3}$$

Here,  $\boldsymbol{\nu}$  denotes the unit outward normal on the surface. Existence and uniqueness of the relaxed micromorphic model using  $X = [H^1(\Omega)]^3 \times [H(\text{curl}, \Omega)]^3$ , where  $[H(\text{curl}, \Omega)]^3$  is to be understood as a row-wise matrix of the vectorial space, is derived in e.g. [33–35]. An example for a function belonging to  $H(\text{curl})$  while not belonging to  $H^1$  is given in Fig. 1.

Although the weak formulation of the relaxed micromorphic model does not represent a mixed formulation and therefore, does not require the use of the commuting de Rham complex for existence and uniqueness in the discrete case, it does introduce the so-called consistent coupling condition [8,36]

$$\mathbf{P} \times \boldsymbol{\nu} = \mathbf{D}\tilde{\mathbf{u}} \times \boldsymbol{\nu} \quad \text{on } \Gamma_D, \tag{2.4}$$

where  $\tilde{\mathbf{u}}$  is the prescribed displacement field on the Dirichlet boundary  $\Gamma_D = \Gamma_D^u = \Gamma_D^p$ . The condition can only be satisfied exactly in the general discrete case, if commuting projections in the sense of a continuous-to-discrete de Rham complex are employed, compare with [37]. Further, when the characteristic length goes to infinity  $L_c \rightarrow \infty$ , a mixed formulation introducing a new variable for the hyperstress  $\mathbf{D} = \mu_{\text{macro}} L_c^2 \text{Curl } \mathbf{P}$  is required to guarantee existence and uniqueness, as shown in [18]. Consequently, the appropriate complex for the relaxed micromorphic model is the classical de Rham complex [38] in three dimensions Fig. 2, where

$$H(\text{div}, \Omega) = \{\mathbf{p} \in [L^2(\Omega)]^3 \mid \text{div } \mathbf{p} \in L^2(\Omega)\}, \quad \text{Div } \mathbf{P} = \begin{bmatrix} \text{div} [P_{11} \ P_{12} \ P_{13}] \\ \text{div} [P_{21} \ P_{22} \ P_{23}] \\ \text{div} [P_{31} \ P_{32} \ P_{33}] \end{bmatrix}, \quad \text{div } \mathbf{p} = \nabla \cdot \mathbf{p}. \tag{2.5}$$

The continuity assumptions on the microdistortion field  $\mathbf{P}$  can be further reduced by taking only its symmetric part  $\text{sym Curl}$  instead of the full  $\text{Curl}$  [21,23–26]

$$[H^1(\Omega)]^3 \xrightarrow{D} [H(\text{curl}, \Omega)]^3 \xrightarrow{\text{Curl}} [H(\text{div}, \Omega)]^3 \xrightarrow{\text{Div}} [L^2(\Omega)]^3$$

**Fig. 2** The classical de Rham exact sequence. The range of each operator is exactly the kernel of the next operator in the sequence, assuming a contractible domain  $\Omega$

$$\begin{aligned}
 I(\mathbf{u}, \mathbf{P}) = & \frac{1}{2} \int_{\Omega} \langle \mathbb{C}_e \text{sym}(\mathbf{D}\mathbf{u} - \mathbf{P}), \text{sym}(\mathbf{D}\mathbf{u} - \mathbf{P}) \rangle + \langle \mathbb{C}_{\text{micro}} \text{sym } \mathbf{P}, \text{sym } \mathbf{P} \rangle \\
 & + \langle \mathbb{C}_c \text{skew}(\mathbf{D}\mathbf{u} - \mathbf{P}), \text{skew}(\mathbf{D}\mathbf{u} - \mathbf{P}) \rangle + \mu_{\text{macro}} L_c^2 \|\text{sym Curl } \mathbf{P}\|^2 dX - \int_{\Omega} \langle \mathbf{u}, \mathbf{f} \rangle \\
 & - \langle \mathbf{P}, \mathbf{M} \rangle dX.
 \end{aligned} \tag{2.6}$$

Since  $\|\text{sym Curl } \mathbf{P}\|^2 \leq \|\text{Curl } \mathbf{P}\|^2$ , this is a considerably weaker formulation than Eq. (2.1).

The appropriate Hilbert space for  $\mathbf{P}$  now reads

$$H(\text{sym Curl}, \Omega) = \{ \mathbf{P} \in [L^2(\Omega)]^{3 \times 3} \mid \text{sym Curl } \mathbf{P} \in [L^2(\Omega)]^{3 \times 3} \}, \quad \text{tr}_{H(\text{sym Curl})} \mathbf{P} = \text{sym}[\mathbf{P} \text{Anti}(\mathbf{v})^T] \Big|_{\partial\Omega}, \tag{2.7}$$

where  $\text{Anti}(\cdot)$  generates the skew symmetric matrix from a vector  $\mathbf{v} \in \mathbb{R}^3$

$$\text{Anti}(\mathbf{v}) = [0 \ -v_3 \ v_2 \ v_3 \ 0 \ -v_1 \ -v_2 \ v_1 \ 0] \in \mathfrak{so}(3), \quad \text{Anti}(\mathbf{v})\mathbf{v} = \mathbf{v} \times \mathbf{v}, \quad \mathbf{v} \in \mathbb{R}^3, \tag{2.8}$$

The existence of minimizers for Problem. 2.6 is shown in [25,26]. The difference in smoothness between  $[H(\text{curl})]^3$  and  $H(\text{sym Curl})$  can be observed when considering spherical matrix fields  $\mathbf{P} = p \mathbb{1} \in \mathbb{R} \cdot \mathbb{1}$

$$\begin{aligned}
 \text{tr}_{H(\text{curl})} \mathbf{P} = \mathbf{P} \text{Anti}(\mathbf{v})^T \Big|_{\partial\Omega} &= p \mathbb{1} \text{Anti}(\mathbf{v})^T \Big|_{\partial\Omega} = p \text{Anti}(\mathbf{v})^T \Big|_{\partial\Omega} \quad \forall \mathbf{P} \in \mathbb{R} \cdot \mathbb{1}, \\
 \text{tr}_{H(\text{sym Curl})} \mathbf{P} = \text{sym}[\mathbf{P} \text{Anti}(\mathbf{v})^T] \Big|_{\partial\Omega} &= \text{sym}[p \text{Anti}(\mathbf{v})^T] \Big|_{\partial\Omega} = 0 \quad \forall \mathbf{P} \in \mathbb{R} \cdot \mathbb{1}.
 \end{aligned} \tag{2.9}$$

The latter identity is evident due to  $p \text{Anti}(\mathbf{v}) \in \mathfrak{so}(3)$  and  $\ker(\text{sym}) = \mathfrak{so}(3)$ . Consequently, the  $H(\text{sym Curl})$  space captures discontinuous spherical tensor fields. A possible interpretation for the kinematics of such a field is depictable under the assumption that the field  $\mathbf{P}$  represents a micro-strain field in the domain. In which case, material points can undergo discontinuous dilatation, see Fig. 3.

This new formulation gives rise to a corresponding complex, designated here the relaxed micromorphic complex, see Fig. 4, where the  $H(\text{div Div})$  space is defined as

$$H(\text{div Div}, \Omega) = \{ \mathbf{P} \in [L^2(\Omega)]^{3 \times 3} \mid \text{div Div } \mathbf{P} \in L^2(\Omega) \}. \tag{2.10}$$

The complex can be seen as an extension of the  $\text{div Div}$ -sequence [27,39], in which only trace-free (deviatoric) gradient fields  $\text{dev } \mathbf{D}\mathbf{u}$  are concerned, where  $\text{dev } \mathbf{X} = \mathbf{X} - \frac{1}{3} \text{tr}(\mathbf{X}) \mathbb{1}$ . In fact, the right half of the complex is the same due to

$$\text{range}(\text{sym Curl dev}) = \text{range}(\text{sym Curl}) \subset \ker(\text{div Div}), \tag{2.11}$$

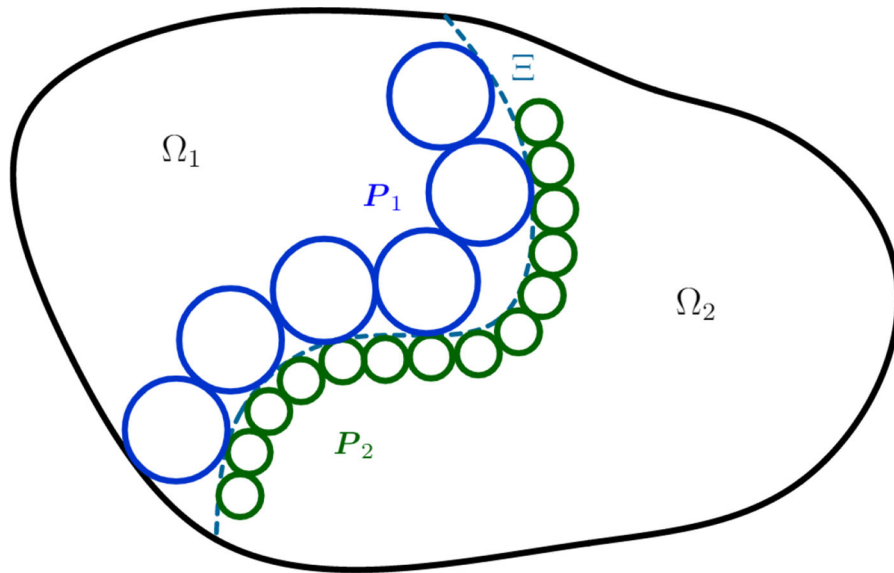


**Fig. 3** Depiction of a field  $\mathbf{P} = \mathbf{P}_1 \cup \mathbf{P}_2 \in H(\text{sym Curl}, \Omega)$ , such that  $\mathbf{P} \notin [H(\text{curl})]^3$ . The circles illustrate the intensity of the spherical part of  $\mathbf{P}$ , which is discontinuous along the dashed line

since (for a full derivation see Appendix A)

$$\text{div Div sym Curl } \mathbf{P} = 0, \tag{2.12}$$

and

$$\text{sym Curl } \mathbf{P} = \text{sym Curl} \left[ \text{dev } \mathbf{P} + \frac{1}{3} \text{tr}(\mathbf{P}) \mathbb{1} \right] = \text{sym Curl dev } \mathbf{P} \quad \forall \mathbf{P} \in \mathbb{R}^{3 \times 3}. \tag{2.13}$$

The left side of the complex [26] is derived from (see Appendix A)

$$\ker(\text{sym Curl}) = D[H^1]^3 \cup \mathbb{R} \cdot \mathbb{1}. \tag{2.14}$$

As shown in [27], the div Div-complex is an exact sequence for a topologically trivial domain. Since the right half of the relaxed micromorphic complex is the same as the right half of the div Div-complex and due to the exactness of Eq. (2.14) as derived in [26], the relaxed micromorphic complex is also an exact sequence for a topologically trivial domain.

*Remark 21* The relaxed micromorphic complex serves to better understand the behaviour of the model with respect to the characteristic length  $L_c$ . Let  $L_c \rightarrow \infty$ , the next space in the sequence  $H(\text{div Div})$  is needed to approximate the hyperstress field

$$\mathbf{D} = \mu_{\text{macro}} L_c^2 \text{sym Curl } \mathbf{P} \in H(\text{div Div}, \Omega) \cap \text{Sym}(3),$$

and to express a stable mixed formulation, compare with [18]. The construction of  $H(\text{div Div})$ -conforming finite elements is beyond the scope of this work.

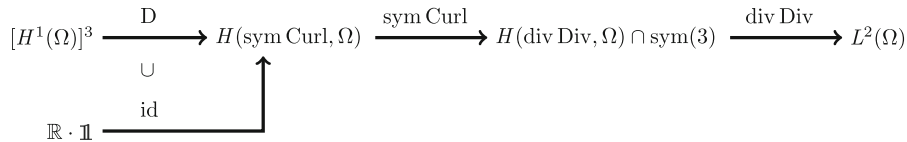


**Fig. 4** The relaxed micromorphic complex for the microdistortion  $\mathbf{P}$  and the corresponding curvature  $\text{sym Curl } \mathbf{P}$ . The kernel  $\ker(H(\text{sym Curl}, \Omega))$  is given fully by gradients of  $D[H^1(\Omega)]^3$  and spherical tensors  $\mathbb{R} \cdot \mathbb{1}$ . The kernel  $\ker(H(\text{div Div}, \Omega))$  is given by  $\text{sym Curl } H(\text{sym Curl}, \Omega)$ . Finally,  $\text{div Div } H(\text{div Div}, \Omega)$  is a surjection onto  $L^2(\Omega)$ . For all these relations we assume a contractible domain

### 3 Abstract variational problem

In order to compare the behaviour of linear finite elements on  $[H^1]^{3 \times 3}$ ,  $[H(\text{curl})]^3$  and  $H(\text{sym Curl})$ , the following abstract variational problem is introduced, drawing characteristics from the relaxed micromorphic model

$$I(\mathbf{P}) = \frac{1}{2} \int_{\Omega} \|\text{sym } \mathbf{P}\|^2 + \|\text{sym Curl } \mathbf{P}\|^2 \, dX - \int_{\Omega} \langle \mathbf{P}, \mathbf{M} \rangle \, dX \rightarrow \min, \tag{3.1}$$

$$\delta I = \int_{\Omega} \langle \text{sym } \mathbf{P}, \text{sym } \delta \mathbf{P} \rangle + \langle \text{sym Curl } \mathbf{P}, \text{sym Curl } (\delta \mathbf{P}) \rangle - \langle \delta \mathbf{P}, \mathbf{M} \rangle \, dX = 0. \tag{3.2}$$

The associated strong form is derived by partial integration

$$\text{sym } \mathbf{P} + \text{Curl}(\text{sym Curl } \mathbf{P}) = \mathbf{M} \quad \text{in } \Omega, \tag{3.3}$$

$$\text{sym}[\mathbf{P} \text{ Anti}(\mathbf{v})^T] = \text{sym}[\tilde{\mathbf{P}} \text{ Anti}(\mathbf{v})^T] \quad \text{on } \Gamma_D, \tag{3.4}$$

$$\text{sym Curl } \mathbf{P} \times \mathbf{v} = 0 \quad \text{on } \Gamma_N, \tag{3.5}$$

where  $\tilde{\mathbf{P}}$  is the prescribed field on the Dirichlet boundary  $\Gamma_D$  and  $\Gamma_N$  represents the Neumann boundary.

*Remark 31* Note that the variational problem resembles a vectorial Maxwell [30] problem  $\mathbf{v} + \text{curl curl } \mathbf{v} = \mathbf{m}$  for some vector field  $\mathbf{v} : \Omega \mapsto \mathbb{R}^3$ . However, in Eq. (3.3) the vectorial rows of  $\mathbf{P}$  are highly coupled and the symmetrization of the Curl operator intervenes.

For a predefined field  $\tilde{\mathbf{P}}$  where the entire boundary is prescribed ( $\partial\Omega = \Gamma_D$ ) the micro-moment  $\mathbf{M}$  is given by

$$\mathbf{M} = \text{sym } \tilde{\mathbf{P}} + \text{Curl}(\text{sym Curl } \tilde{\mathbf{P}}), \tag{3.6}$$

and the analytical solution is  $\mathbf{P} = \tilde{\mathbf{P}}$ . Due to the generalized Korn’s inequality [23–26,40,41], the variational problem Eq. (3.1) and the weak form Eq. (3.2) are well-posed in the space  $H(\text{sym Curl}, \Omega)$ .

### 4 Finite element formulations

In the following we introduce finite elements using Voigt notation. As a result, the microdistortion and micro-moment fields  $\mathbf{P}$  and  $\mathbf{M}$  are given by nine-dimensional vectors and the symmetry by the nine-by-nine matrix  $\mathbb{S}$

$$\mathbf{P} = [P_{11} \ P_{12} \ P_{13} \ P_{21} \ P_{22} \ P_{23} \ P_{31} \ P_{32} \ P_{33}]^T, \quad \mathbf{P}, \mathbf{M} \in \mathbb{R}^9, \mathbb{S} \in \mathbb{R}^{9 \times 9}. \tag{4.1}$$

All formulations apply to a linear tetrahedral element with a barycentric mapping (see Fig. 5)

$$\mathbf{x}(\xi, \eta, \zeta) = (1 - \xi - \eta - \zeta) \mathbf{x}_1 + \xi \mathbf{x}_1 + \eta \mathbf{x}_2 + \zeta \mathbf{x}_3, \quad \mathbf{J} = D\mathbf{x} = [\mathbf{x}_2 - \mathbf{x}_1 \ \mathbf{x}_3 - \mathbf{x}_1 \ \mathbf{x}_4 - \mathbf{x}_1], \tag{4.2}$$

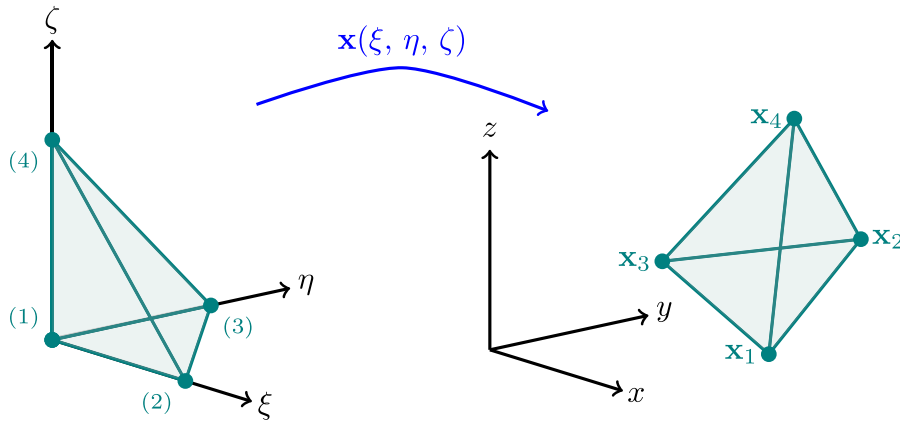


**Fig. 5** Affine mapping from the reference element to the physical domain

where  $J$  is the Jacobi matrix.

#### 4.1 Lagrangian $[H^1]^{3 \times 3}$ -element

The functionals of Lagrangian finite elements are defined by point-wise evaluation

$$l_i(u) \Big|_{x_j} = \delta_{ij} u \Big|_{x_j}, \tag{4.3}$$

where  $\delta_{ij}$  is the Kronecker delta. For the construction of the linear Lagrangian element, the evaluation of the degrees of freedom for the polynomial space  $P^1 = \text{span}\{1, \xi, \eta, \zeta\}$  on the reference element yields the same barycentric base functions used for the element mapping

$$n_1(\xi, \eta, \zeta) = 1 - \xi - \eta - \zeta, \quad n_2(\xi, \eta, \zeta) = \xi, \tag{4.4}$$

$$n_3(\xi, \eta, \zeta) = \eta, \quad n_4(\xi, \eta, \zeta) = \zeta. \tag{4.5}$$

The entire ansatz matrix for the interpolation of a nine-dimensional vector can be built accordingly

$$N = [n_1 \mathbb{1}_9 \quad n_2 \mathbb{1}_9 \quad n_3 \mathbb{1}_9 \quad n_4 \mathbb{1}_9] \in \mathbb{R}^{9 \times 36}, \quad \mathbb{1}_9 \in \mathbb{R}^{9 \times 9}, \quad [\mathbb{1}_9]_{ij} = \delta_{ij}, \quad i, j \in \{1, 2, \dots, 9\}, \tag{4.6}$$

where  $\mathbb{1}_9$  is the nine-dimensional unit matrix. The curl of a row of  $P$  with respect to the physical domain is retrieved following the standard chain rule

$$\text{curl}_x \mathbf{p}_i = J^{-T} \text{curl}_\xi \mathbf{p}_i = J^{-T} \text{Anti}(\nabla_\xi) \mathbf{p}_i. \tag{4.7}$$

The matrix Curl operator is defined by the row-wise application of the curl operator. The resulting element stiffness matrix reads

$$\mathbf{K}_{\text{lag}} = \int_{\Omega} (N^T \mathbb{S} N + \text{Curl}(N)^T \mathbb{S} \text{Curl} N) dX \in \mathbb{R}^{36 \times 36}, \tag{4.8}$$

where  $\mathbb{S}$  defines the equivalent matrix symmetry operator in Voigt notation. The Lagrangian element belongs to  $\mathcal{L}^1 \subset H^1$  and its interpolant produces the error estimate

$$\|u - \Pi_{\mathcal{L}} u\|_{L^2} \leq h^2 |u|_{H^2}, \tag{4.9}$$

where  $u$  is the exact solution,  $\Pi_{\mathcal{L}}$  is the Lagrangian interpolant and  $h$  is a measure of the element’s size.

#### 4.2 Nédélec $[H(\text{curl})]^3$ -element

Nédélec [28] finite elements are conforming in  $H(\text{curl})$ . This is achieved by controlling the tangential projections of the base functions on the edges of a finite element. The lowest degrees of freedom, namely edge type, are defined as integrals along the curve of the element’s edge

$$l_{ij}(\mathbf{p}) = \int_{s_i} q_j(\mathbf{p}, \boldsymbol{\tau}) \, ds \quad \forall q_j \in P^{p-1}(s_i). \tag{4.10}$$

Here  $q_j$  are test functions. The adequate polynomial space is defined in [28] as

$$R^p = [P^{p-1}]^3 \oplus S^p, \quad S^p = \{\mathbf{p} \in [\tilde{P}^p]^3 \mid \langle \mathbf{p}, \mathbf{x} \rangle = 0\}, \tag{4.11}$$

where  $\tilde{P}$  is the space of homogeneous polynomials. For linear polynomials  $p = 1$  the space reads

$$R^1 = \text{span} \left\{ \begin{bmatrix} 1 \\ 0 \\ 0 \end{bmatrix}, \begin{bmatrix} 0 \\ 1 \\ 0 \end{bmatrix}, \begin{bmatrix} 0 \\ 0 \\ 1 \end{bmatrix}, \begin{bmatrix} 0 \\ \zeta \\ -\eta \end{bmatrix}, \begin{bmatrix} -\zeta \\ 0 \\ \xi \end{bmatrix}, \begin{bmatrix} \eta \\ -\xi \\ 0 \end{bmatrix} \right\}, \quad \dim R^1 = 6. \tag{4.12}$$

The latter describes the polynomial space for linear Nédélec elements of the first type  $\mathcal{N}_I^0$ . Evaluating the degrees of freedom on the reference tetrahedron using the test functions  $q_j = 1$  yields the corresponding base functions (see Fig. 6)

$$\begin{aligned} \boldsymbol{\vartheta}_1 &= \begin{bmatrix} 1 - \eta - \zeta \\ \xi \\ \xi \end{bmatrix}, & \boldsymbol{\vartheta}_2 &= \begin{bmatrix} -\eta \\ \xi \\ 0 \end{bmatrix}, & \boldsymbol{\vartheta}_3 &= \begin{bmatrix} \eta \\ 1 - \xi - \zeta \\ \eta \end{bmatrix}, \\ \boldsymbol{\vartheta}_4 &= \begin{bmatrix} \zeta \\ \zeta \\ 1 - \xi - \eta \end{bmatrix}, & \boldsymbol{\vartheta}_5 &= \begin{bmatrix} -\zeta \\ 0 \\ \xi \end{bmatrix}, & \boldsymbol{\vartheta}_6 &= \begin{bmatrix} 0 \\ -\zeta \\ \eta \end{bmatrix}. \end{aligned} \tag{4.13}$$

*Remark 41* The zero power notation of the space  $\mathcal{N}_I^0$  reminds that the base functions generate constant tangential projections on the edge. An alternative construction using the full polynomial space is given by the Nédélec elements of the second type  $\mathcal{N}_{II}^1$  [29].

The base functions are vectors defined on the reference element. In order to map them to the physical domain we employ the covariant Piola transformation

$$\boldsymbol{\theta}_i = \mathbf{J}^{-T} \boldsymbol{\vartheta}_i. \tag{4.14}$$



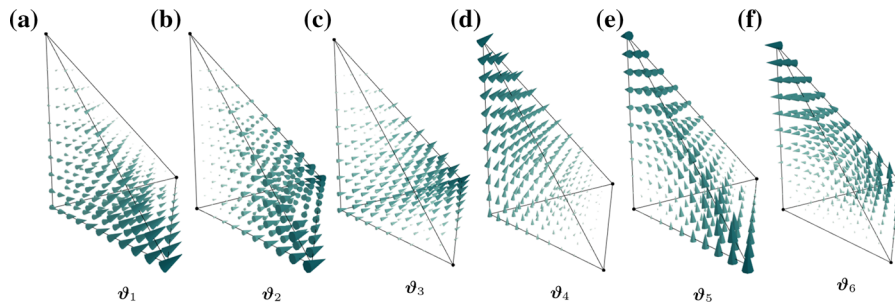


**Fig. 6** Linear Nédélec base functions on the reference tetrahedron

Further, the curl of vectors undergoing a covariant Piola mapping is given by the contravariant Piola transformation

$$\text{curl}_x \theta_i = \frac{1}{\det \mathbf{J}} \mathbf{J} \text{curl}_\xi \vartheta_i. \tag{4.15}$$

*Remark 42* Note that Piola transformations guarantee a consistent projection on the element’s boundaries in terms of size. However, the transformation does not control whether the tangential projections of neighbouring elements are parallel or anti-parallel, since the vectorial base functions are mapped to the physical domain separately by the corresponding Jacobi matrix of each element. Consequently, a correction function is employed to assert consistency, compare with [18].

For the construction of the finite element we define a corresponding ansatz matrix

$$\Theta = \begin{bmatrix} \theta_1 & \mathbf{0} & \mathbf{0} & \theta_2 & \mathbf{0} & \mathbf{0} & \theta_3 & \mathbf{0} & \mathbf{0} & \theta_4 & \mathbf{0} & \mathbf{0} & \theta_5 & \mathbf{0} & \mathbf{0} & \theta_6 & \mathbf{0} & \mathbf{0} \\ \mathbf{0} & \theta_1 & \mathbf{0} & \mathbf{0} & \theta_2 & \mathbf{0} & \mathbf{0} & \theta_3 & \mathbf{0} & \mathbf{0} & \theta_4 & \mathbf{0} & \mathbf{0} & \theta_5 & \mathbf{0} & \mathbf{0} & \theta_6 & \mathbf{0} \\ \mathbf{0} & \mathbf{0} & \theta_1 & \mathbf{0} & \mathbf{0} & \theta_2 & \mathbf{0} & \mathbf{0} & \theta_3 & \mathbf{0} & \mathbf{0} & \theta_4 & \mathbf{0} & \mathbf{0} & \theta_5 & \mathbf{0} & \mathbf{0} & \theta_6 \end{bmatrix} \in \mathbb{R}^{9 \times 18}, \tag{4.16}$$

where  $\mathbf{0} = [0 \ 0 \ 0]^T$  is a three-dimensional vector of zeros. The Curl of the microdistortion  $\mathbf{P}$  is calculated using Eq. (4.15) for each base function

$$\text{Curl } \Theta = \begin{bmatrix} \text{curl } \theta_1 & \mathbf{0} & \mathbf{0} & \dots & \text{curl } \theta_6 & \mathbf{0} & \mathbf{0} \\ \mathbf{0} & \text{curl } \theta_1 & \mathbf{0} & \dots & \mathbf{0} & \text{curl } \theta_6 & \mathbf{0} \\ \mathbf{0} & \mathbf{0} & \text{curl } \theta_1 & \dots & \mathbf{0} & \mathbf{0} & \text{curl } \theta_6 \end{bmatrix} \in \mathbb{R}^{9 \times 18}. \tag{4.17}$$

Consequently, the element stiffness matrix reads

$$\mathbf{K}_{\text{néd}} = \int_{\Omega} (\Theta^T \mathbb{S} \Theta + \text{Curl}(\Theta)^T \mathbb{S} \text{Curl } \Theta) dX \in \mathbb{R}^{18 \times 18}. \tag{4.18}$$

The Nédélec element belongs to the subspace  $\mathcal{N}_I^0 \subset H(\text{curl})$ . The corresponding interpolant yields the following error estimate

$$\|\mathbf{v} - \Pi_{\mathcal{N}} \mathbf{v}\|_{L^2} \leq h |\mathbf{v}|_{H^1}, \tag{4.19}$$

where  $\mathbf{v}$  is the exact solution,  $\Pi_{\mathcal{N}}$  is the Nédélec interpolant and  $h$  is a measure of the element’s size.

### 4.3 The $H(\text{sym Curl})$ -element

Due to the following inclusion the two former finite element formulations are possible candidates for computations in  $H(\text{sym Curl})$ . However, as denoted by the trace in Eq. (2.9) and shown in [26], the  $H(\text{sym Curl})$  space is strictly larger

$$[H^1]^{3 \times 3} \subset [H(\text{curl})]^3 \subset H(\text{sym Curl}). \tag{4.20}$$

Consequently, there can exist solutions that belong to  $H(\text{sym Curl})$  while not belonging to  $[H(\text{curl})]^3$ , as demonstrated in Sect. 5.3. For the design of an  $H(\text{sym Curl})$ -conforming finite element [32], the trace must vanish on the interface of neighbouring elements. In other words, a function  $\mathbf{P}$  belongs to  $H(\text{sym Curl})$  if

$$\llbracket \text{tr}_{H(\text{sym Curl})}(\mathbf{P}) \rrbracket \Big|_{\Xi_i} = 0 \quad \forall \Xi_i \text{ in } \Omega, \tag{4.21}$$

where  $\llbracket \cdot \rrbracket$  represents the jump operator and  $\Xi_i$  is an interface between neighbouring elements. The trace condition can be reconstructed as

$$\text{sym}[\mathbf{P} \text{ Anti}(\mathbf{v})^T] = 0 \iff \langle \mathbf{P} \text{ Anti}(\mathbf{v})^T, \mathbf{S}_i \rangle = 0 \quad \forall \mathbf{S}_i \in \text{Sym}(3). \tag{4.22}$$

A simple basis for  $\text{Sym}(3)$  is given by the symmetric decomposition of a matrix filled with ones ( $\mathbf{A} = \sum_i \sum_j \mathbf{1} \mathbf{e}_i \otimes \mathbf{e}_j$ )

$$\text{Sym}(3) = \text{span}\{\mathbf{e}_1 \otimes \mathbf{e}_1, \mathbf{e}_2 \otimes \mathbf{e}_2, \mathbf{e}_3 \otimes \mathbf{e}_3, \text{sym}(\mathbf{e}_1 \otimes \mathbf{e}_2), \text{sym}(\mathbf{e}_1 \otimes \mathbf{e}_3), \text{sym}(\mathbf{e}_2 \otimes \mathbf{e}_3)\}. \tag{4.23}$$

Accordingly, any affine transformation  $\mathbf{F}$  that maps to linearly independent vectors allows to generalize the basis

$$\text{Sym}(3) = \text{span}\{\mathbf{F} \mathbf{e}_1 \otimes \mathbf{e}_1 \mathbf{F}^T, \dots, \text{sym}(\mathbf{F} \mathbf{e}_2 \otimes \mathbf{e}_3 \mathbf{F}^T)\}, \quad \mathbf{F} \in \text{GL}(3). \tag{4.24}$$

Clearly, the transformation leaves the symmetry invariant. Defining  $\mathbf{a} \in \mathbb{R}^3, \mathbf{b} \in \mathbb{R}^3$  such that  $\mathbf{F} = [\mathbf{a} \ \mathbf{b} \ \mathbf{v}] \in \text{GL}(3)$ , where  $\mathbf{v}$  is a normal on an element's face, we observe that five conditions instead of six suffice to assert Eq. (4.22) since

$$\langle \mathbf{P} \text{ Anti}(\mathbf{v})^T, \mathbf{v} \otimes \mathbf{v} \rangle = \langle \mathbf{P}, \mathbf{v} \otimes \mathbf{v} \text{ Anti}(\mathbf{v}) \rangle = \langle \mathbf{P}, \mathbf{v} \otimes \mathbf{v} \times \mathbf{v} \rangle = 0, \tag{4.25}$$

is always satisfied. In other words, five conditions control whether  $\mathbf{P}$  is point-wise  $H(\text{sym Curl})$ -conforming on a face

$$\begin{aligned} \langle \mathbf{P} \text{ Anti}(\mathbf{v})^T, \mathbf{a} \otimes \mathbf{a} \rangle &= 0, & \langle \mathbf{P} \text{ Anti}(\mathbf{v})^T, \mathbf{b} \otimes \mathbf{b} \rangle &= 0, & \langle \mathbf{P} \text{ Anti}(\mathbf{v})^T, \text{sym}(\mathbf{a} \otimes \mathbf{b}) \rangle &= 0, \\ \langle \mathbf{P} \text{ Anti}(\mathbf{v})^T, \text{sym}(\mathbf{a} \otimes \mathbf{v}) \rangle &= 0, & \langle \mathbf{P} \text{ Anti}(\mathbf{v})^T, \text{sym}(\mathbf{b} \otimes \mathbf{v}) \rangle &= 0. \end{aligned} \tag{4.26}$$

Yet, these are not enough conditions to fully identify an element of  $\mathbb{R}^{3 \times 3}$ . The remaining conditions can be defined as

$$\begin{aligned} \langle \mathbf{P}, \mathbf{b} \otimes (\mathbf{a} \times \mathbf{v}) - \mathbf{a} \otimes (\mathbf{b} \times \mathbf{v}) \rangle &= 0, & \langle \mathbf{P}, \mathbf{a} \otimes \mathbf{v} \rangle &= 0, \\ \langle \mathbf{P}, \mathbf{b} \otimes \mathbf{v} \rangle &= 0, & \langle \mathbf{P}, \mathbf{v} \otimes \mathbf{v} \rangle &= 0, \end{aligned} \tag{4.27}$$

which, together with the trace conditions, determine the element uniquely. Note that the latter identities are all in  $\ker(\text{tr}_{H(\text{sym Curl})})$  due to  $\mathbf{v} \times \mathbf{v} = 0$  and are therefore linearly independent of the trace conditions. To see their linear independence from one another, simply map back to the Cartesian basis with  $\mathbf{F}^{-1}$ .

The conditions in Eq. (4.26) ensure conformity on a face. On an edge two faces meet and the conditions must be satisfied for both. On each edge we define  $\mathbf{a} = \boldsymbol{\tau}$ ,  $\mathbf{b} = \boldsymbol{\gamma}_i = \boldsymbol{\tau} \times \mathbf{v}_i$ , where  $\boldsymbol{\tau}$  is the edge tangent,  $\mathbf{v}_i$  is the normal on face  $i$  and  $\boldsymbol{\gamma}_i$  is the corresponding conormal. Considering the following identity

$$\mathbf{v}_1 \times \boldsymbol{\gamma}_1 = \mathbf{v}_2 \times \boldsymbol{\gamma}_2 = \boldsymbol{\tau}, \tag{4.28}$$

the conditions for conformity can be reformulated as

$$\begin{aligned} \langle \mathbf{P}, \boldsymbol{\tau} \otimes \boldsymbol{\gamma}_i \rangle = 0, \quad \langle \mathbf{P}, \boldsymbol{\tau} \otimes \boldsymbol{\tau} + \boldsymbol{\gamma}_i \otimes \boldsymbol{\gamma}_i \rangle = 0, \quad \langle \mathbf{P}, \mathbf{v}_i \otimes \boldsymbol{\gamma}_i \rangle = 0, \quad i = \{1, 2\}, \\ \langle \mathbf{P}, \boldsymbol{\tau} \otimes \boldsymbol{\rho}_1 \rangle = 0, \quad \langle \mathbf{P}, \boldsymbol{\tau} \otimes \boldsymbol{\rho}_2 \rangle = 0, \end{aligned} \tag{4.29}$$

where  $\boldsymbol{\rho}_1$  and  $\boldsymbol{\rho}_2$  are two arbitrary vectors spanning the surface orthogonal to  $\boldsymbol{\tau}$ . The upper conditions allow to determine eight terms of  $\mathbf{P}$ . One term remains to be determined using

$$\langle \mathbf{P}, \boldsymbol{\tau} \otimes \boldsymbol{\tau} \rangle = 0, \tag{4.30}$$

which controls multiples of the identity matrix. The conditions are linearly independent as long as  $\mathbf{v}_1 \not\parallel \mathbf{v}_2$ .

The same methodology may be used to construct vertex conformity and uniqueness conditions. However, for an unstructured mesh it is unclear how to do this in a way that is independent of the geometry. Consequently, at the vertices we impose full continuity with the exception of the identity

$$\begin{aligned} P_{12}, P_{13}, P_{21}, P_{23}, P_{31}, P_{32} = 0, \quad P_{11} - P_{22} = 0, \quad P_{22} - P_{33} = 0, \\ \text{tr } \mathbf{P} = \langle \mathbf{P}, \mathbb{1} \rangle = P_{11} + P_{22} + P_{33} = 0, \end{aligned} \tag{4.31}$$

where the conditions in the upper row assert conformity and the trace controls the identity matrix.

Unlike for the previous elements that were constructed in the reference domain, the construction of the  $H(\text{sym Curl})$ -element is done directly on the grid using the degrees of freedom from Eq. (4.31). We reformulate the degrees of freedom for the linear element as vector operators

$$\begin{aligned} P_{11} - P_{22} : \quad \mathbf{I}_1 = [1 \ 0 \ 0 \ 0 \ -1 \ 0 \ 0 \ 0 \ 0], \quad P_{22} - P_{33} : \quad \mathbf{I}_5 = [0 \ 0 \ 0 \ 0 \ 1 \ 0 \ 0 \ 0 \ -1], \\ \text{tr } \mathbf{P} : \quad \mathbf{I}_9 = [1 \ 0 \ 0 \ 0 \ 1 \ 0 \ 0 \ 0 \ 1], \quad P_{ij} \text{ s.t. } i \neq j : \quad \mathbf{I}_i = \mathbf{e}_i^T, \quad i \in \{2, 3, 4, 6, 7, 8\}, \end{aligned} \tag{4.32}$$

where  $\mathbf{e}_i$  is the unit vector in  $\mathbb{R}^9$ . Consequently, the collection of the degrees of freedom can be defined as the operator matrix

$$\mathbf{L} = [\mathbf{I}_1^T \quad \mathbf{I}_2^T \quad \mathbf{I}_3^T \quad \mathbf{I}_4^T \quad \mathbf{I}_5^T \quad \mathbf{I}_6^T \quad \mathbf{I}_7^T \quad \mathbf{I}_8^T \quad \mathbf{I}_9^T]^T \in \mathbb{R}^{9 \times 9}. \tag{4.33}$$

The ansatz matrix is given by the monomial basis

$$\mathbf{X} = [1 \ \mathbb{1}_9 \quad x \ \mathbb{1}_9 \quad y \ \mathbb{1}_9 \quad z \ \mathbb{1}_9] \in \mathbb{R}^{9 \times 36}, \quad \mathbb{1}_9 \in \mathbb{R}^{9 \times 9}. \tag{4.34}$$

In order to construct the corresponding base functions, the product  $\mathbf{L} \mathbf{X}$  is evaluated at each node of a finite element

$$\mathbf{C}^{-1} = \left[ (\mathbf{L} \mathbf{X})^T \Big|_{n_1} \quad (\mathbf{L} \mathbf{X})^T \Big|_{n_2} \quad (\mathbf{L} \mathbf{X})^T \Big|_{n_3} \quad (\mathbf{L} \mathbf{X})^T \Big|_{n_4} \right]^T \in \mathbb{R}^{36 \times 36}, \tag{4.35}$$

where every column of  $\mathbf{C}$  gives the constant factors for one base function. Therefore, the resulting local basis is given by

$$\mathbf{B} = \mathbf{X} \mathbf{C} \in \mathbb{R}^{9 \times 36}, \quad \mathbf{P} = \bigcup_{e=1}^{n_{\text{elements}}} \mathbf{B} \mathbf{P}_e. \tag{4.36}$$

In order to find the Curl of  $\mathbf{P}$ , we redefine the operator in Voigt notation

$$\text{Curl } \mathbf{P} = \begin{bmatrix} \text{Anti}(\nabla) & \mathbf{O} & \mathbf{O} \\ \mathbf{O} & \text{Anti}(\nabla) & \mathbf{O} \\ \mathbf{O} & \mathbf{O} & \text{Anti}(\nabla) \end{bmatrix} \mathbf{P}, \quad \text{Anti}(\nabla) = \begin{bmatrix} 0 & -\partial_3 & \partial_2 \\ \partial_3 & 0 & -\partial_1 \\ -\partial_2 & \partial_1 & 0 \end{bmatrix}, \quad \mathbf{O} = \begin{bmatrix} 0 & 0 & 0 \\ 0 & 0 & 0 \\ 0 & 0 & 0 \end{bmatrix}. \tag{4.37}$$

Consequently, the Curl of the base functions is given by

$$\text{Curl } \mathbf{B} = (\text{Curl } \mathbf{X}) \mathbf{C}. \tag{4.38}$$

The element stiffness matrix can now be defined as

$$\mathbf{K}_{\text{sym}} = \int_{\Omega} (\mathbf{B}^T \mathbb{S} \mathbf{B} + \text{Curl}(\mathbf{B})^T \mathbb{S} \text{Curl } \mathbf{B}) \, dX \in \mathbb{R}^{36 \times 36}. \tag{4.39}$$

*Remark 43* At the construction of the local–global map, eight of the nine degrees of freedom on a node are shared by neighbouring elements. The ninth degree is built locally for each element and is not connected over the element’s boundaries. With this characteristic, the lower continuity of the space is made possible.

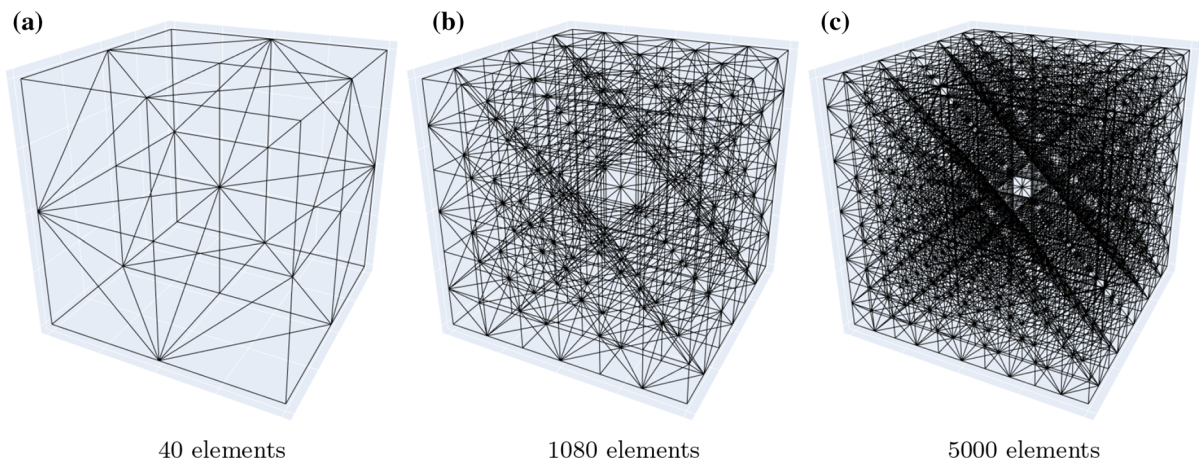


**Fig. 7** Finite element meshes from 40 to 5000 elements for the domain  $\Omega = [-1, 1]^3$

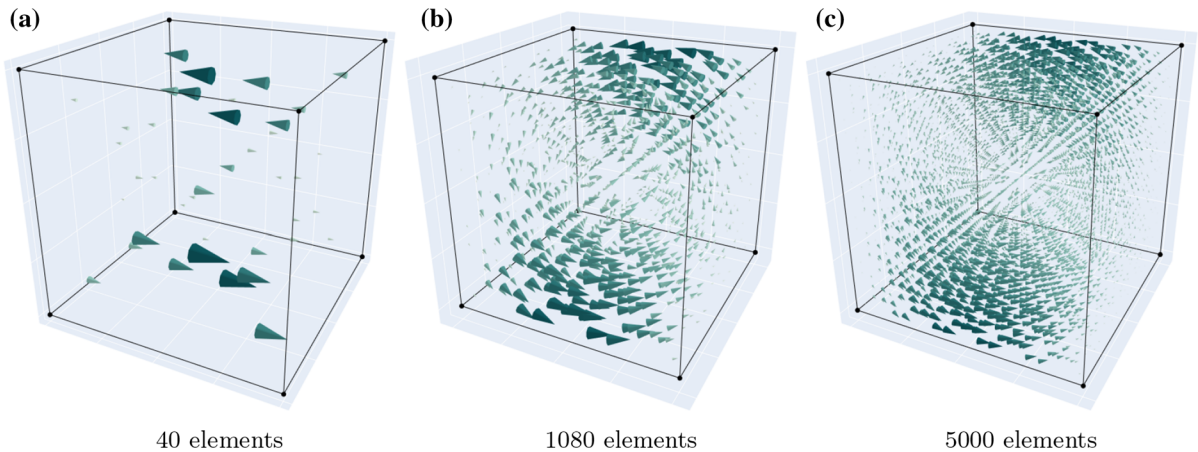


**Fig. 8** Vortex field for various discretizations of the  $H(\text{sym Curl})$ -element displaying the first row of  $\mathbf{P}$

The element belongs to  $\mathcal{T}^1 \subset H(\text{sym Curl})$  and its interpolant produces the standard Lagrangian error estimate (see [32])

$$\|\mathbf{T} - \Pi_{\mathcal{T}}\mathbf{T}\|_{L^2} \leq h^2 |\mathbf{T}|_{H^2}, \tag{4.40}$$

where  $\mathbf{T}$  is the exact solution tensor,  $\Pi_{\mathcal{T}}$  is the interpolant and  $h$  is a measure of the element’s size.

### 5 Numerical examples

In the following we test the convergence of the three finite element formulations against various simple analytical solutions. For all formulations we make use of the cube  $\Omega = [-1, 1]^3$ . The finite element meshes range from 40 to 5000 elements, see Fig. 7.

We measure convergence in the Lebesgue  $L^2$ -norm

$$\|\tilde{\mathbf{P}} - \mathbf{P}\|_{L^2} = \sqrt{\int_{\Omega} \|\tilde{\mathbf{P}} - \mathbf{P}\|_F^2 dX}, \tag{5.1}$$

and the  $H(\text{sym Curl})$ -norm

$$\|\tilde{\mathbf{P}} - \mathbf{P}\|_{H(\text{sym Curl})} = \sqrt{\|\tilde{\mathbf{P}} - \mathbf{P}\|_{L^2}^2 + \int_{\Omega} \|\text{sym Curl}(\tilde{\mathbf{P}} - \mathbf{P})\|_F^2 dX}. \tag{5.2}$$

#### 5.1 Smooth solution field

In the first example we set the microdistortion to

$$\tilde{\mathbf{P}} = (1 - x)(1 + x) \begin{bmatrix} -y - z & x & x \\ -y - z & x & x \\ -y - z & x & x \end{bmatrix}. \tag{5.3}$$

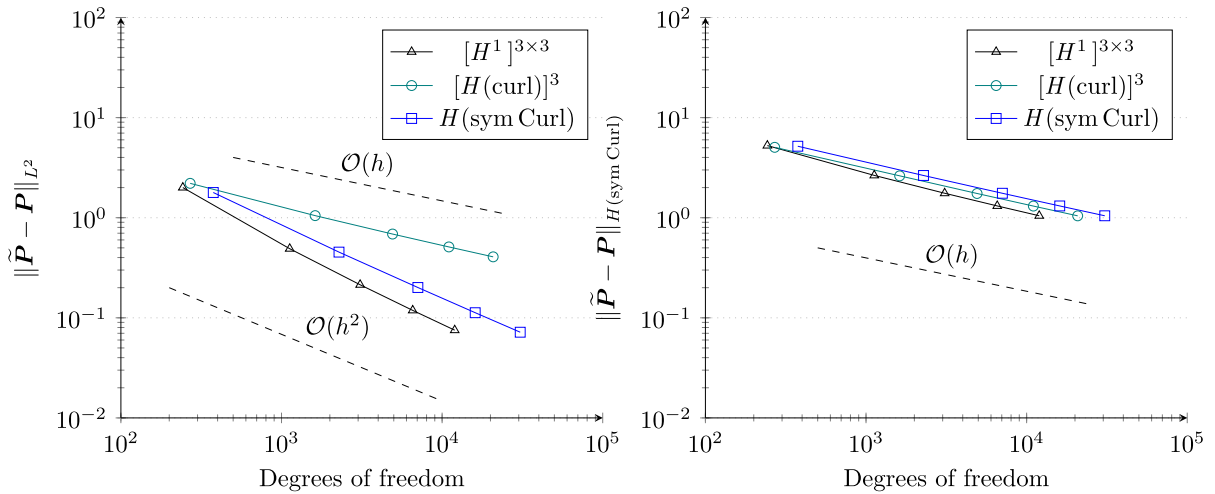


**Fig. 9** Convergence rates for the rotational benchmark

Effectively, the microdistortion is now a vortex field that must vanish at  $x = -1$  and  $x = 1$ , see Fig. 8. Since the microdistortion is clearly continuous, it is an element of  $[H^1]^{3 \times 3}$ . The microdistortion field gives rise to the micro-moment

$$\mathbf{M} = \begin{bmatrix} x^2y + x^2z - y - z & 0.5(x^2y - x^3 + x^2z + 9x - y - z) & 0.5(x^2y - x^3 + x^2z + 9x - y - z) \\ 0.5(x^2y - x^3 + x^2z + x - y - z) & -x^3 + x & -x^3 + 9x \\ 0.5(x^2y - x^3 + x^2z + x - y - z) & -x^3 + 9x & -x^3 + x \end{bmatrix}. \tag{5.4}$$

The convergence rates are given in Fig. 9. In the  $L^2$ -norm, the Nédélec element converges linearly, whereas the Lagrangian element and the  $H(\text{sym Curl})$ -element converge quadratically, as expected for smooth fields. All three formulations converge linearly in the  $H(\text{sym Curl})$ -norm.

### 5.2 Discontinuous normal trace

In the following benchmark we define the discontinuous microdistortion field

$$\tilde{\mathbf{P}} = \begin{cases} \begin{bmatrix} 1 & 0 & 0 \\ 0 & 0 & 0 \\ 0 & 0 & 0 \end{bmatrix} & \text{for } x < 0, \\ 0 & \text{otherwise.} \end{cases} \tag{5.5}$$

The latter field belongs to  $[H(\text{curl})]^3$  but not to  $[H^1]^{3 \times 3}$ . This is because only the normal projection of the microdistortion  $\mathbf{P}$  is discontinuous with regard to the unit vector  $\mathbf{e}_1 = [1 \ 0 \ 0]^T$

$$\text{tr}_{H(\text{curl})} \mathbf{P} \Big|_{\Gamma_1} = \mathbf{P} \text{Anti}(\mathbf{e}_1)^T = 0, \quad \Gamma_1 \perp \mathbf{e}_1. \tag{5.6}$$

The corresponding micro-moments are clearly

$$\mathbf{M} = \tilde{\mathbf{P}}. \tag{5.7}$$

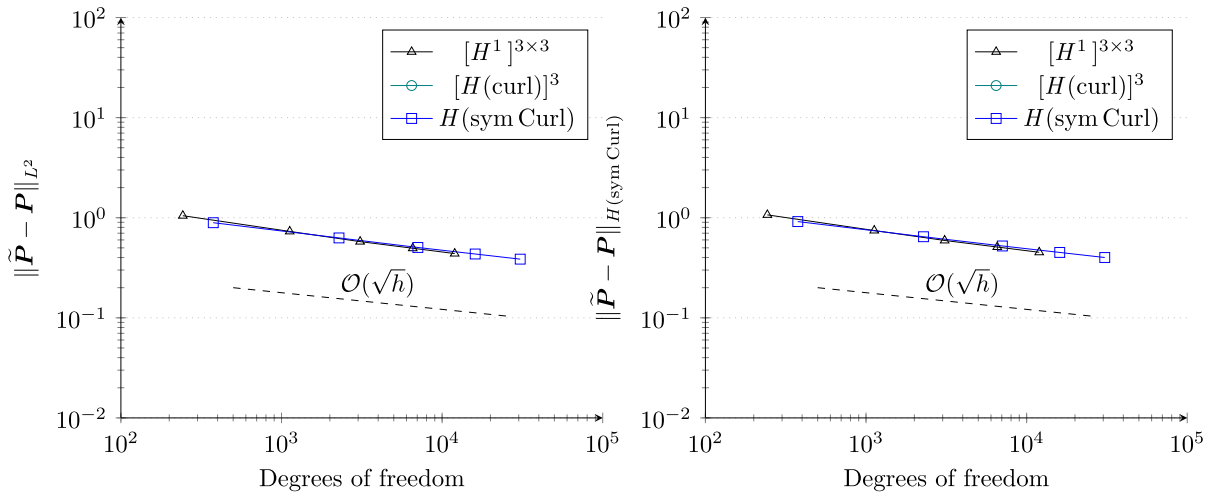


**Fig. 10** Convergence for the discontinuous normal projection benchmark

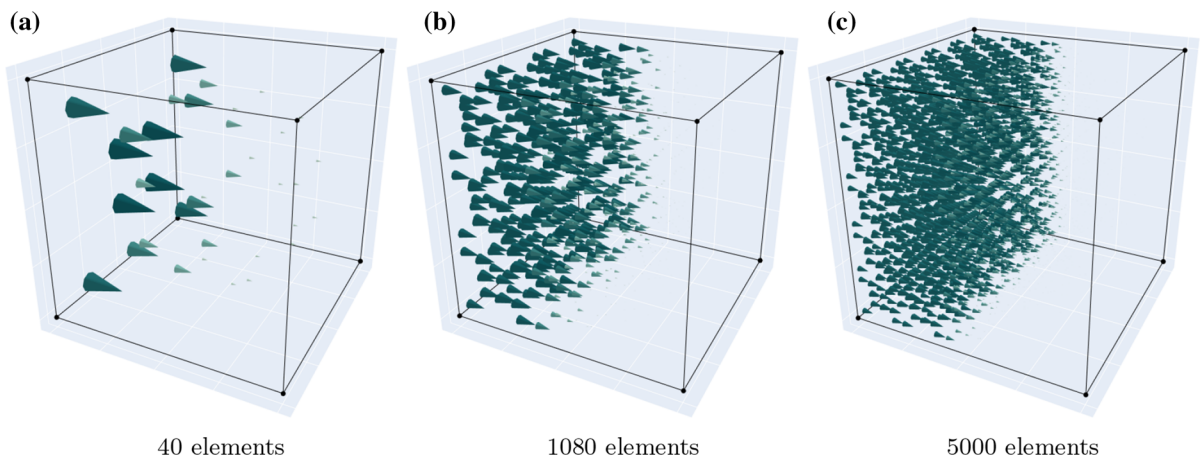


**Fig. 11** Discontinuous normal projection for various discretizations of the  $H^1$ -element displaying the first row of  $P$

The approximation captured by the various discretizations is depicted in Fig. 11, Fig. 12 and Fig. 13. The noise (small vectors in  $x > 0$ ) in the solution is apparent for the Lagrangian- and  $H(\text{sym Curl})$ -formulations. The convergence rates are given in Fig. 10. The Nédélec element finds the analytical solution immediately for all discretizations. Both the Lagrangian formulation and the  $H(\text{sym Curl})$ -formulation converge sub-optimally. In case of the  $H(\text{sym Curl})$ -formulation this is due to the higher continuity imposed at the vertices. Despite appearing similar, the values of the convergence in the  $L^2$ -norm are not equal to the values of the convergence in the  $H(\text{sym Curl})$ -norm. However, the difference is small.

### 5.3 Discontinuous identity

In the last benchmark we test the behaviour of a discontinuous identity microdistortion field

$$\tilde{P} = \begin{cases} \mathbb{1} & \text{for } x < 0 \\ 0 & \text{otherwise} \end{cases}, \tag{5.8}$$

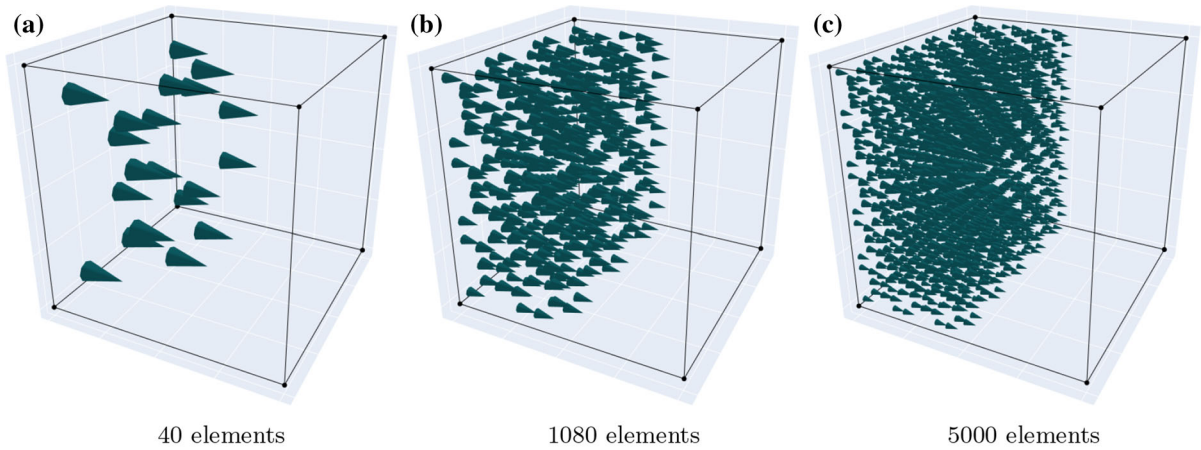


**Fig. 12** Discontinuous normal projection for various discretizations of the  $H(\text{curl})$ -element displaying the first row of  $\mathbf{P}$

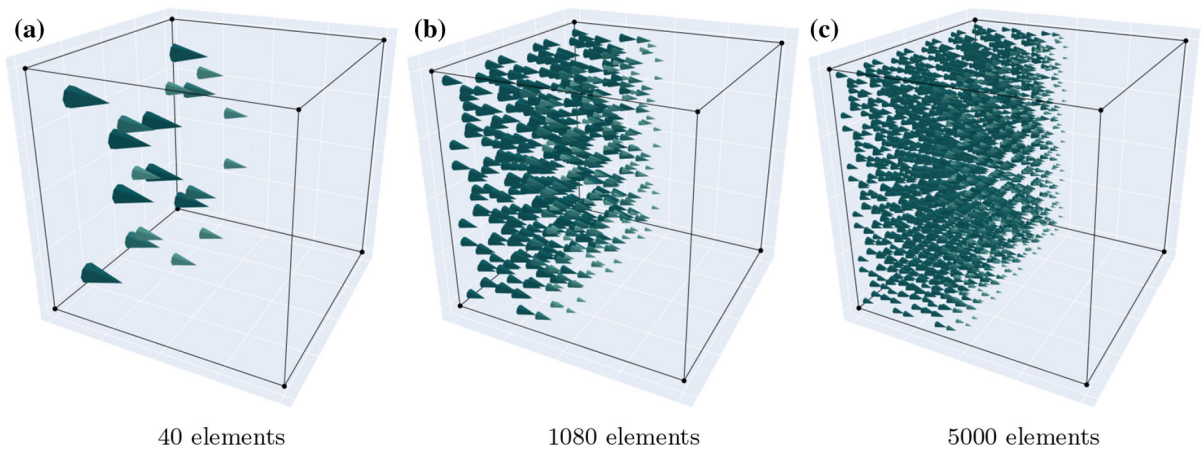


**Fig. 13** Discontinuous normal projection for various discretizations of the  $H(\text{sym Curl})$ -element displaying the first row of  $\mathbf{P}$

for which the micro-moment reads

$$\mathbf{M} = \widetilde{\mathbf{P}}. \tag{5.9}$$

Clearly the solution is in  $H(\text{sym Curl})$  but not in  $[H(\text{curl})]^3$  or  $[H^1]^{3 \times 3}$  since

$$\begin{aligned} \text{tr}_{H(\text{curl})} \mathbf{P} \Big|_{\Gamma_1} &= \begin{cases} \text{Anti}(\mathbf{e}_1)^T & \text{for } x < 0 \\ 0 & \text{otherwise} \end{cases}, \\ \text{tr}_{H(\text{sym Curl})} \mathbf{P} \Big|_{\Gamma_1} &= 0, \end{aligned} \tag{5.10}$$

where  $\mathbf{e}_1 = [1 \ 0 \ 0]^T$  and  $\Gamma_1 \perp \mathbf{e}_1$ .

As shown in Fig. 14, the  $H(\text{sym Curl})$ -formulation finds the analytical solution immediately for all domain discretizations, whereas the  $H^1$  and  $H(\text{curl})$  formulations exhibit sub-optimal square root convergence. However, in the  $H(\text{sym Curl})$ -norm only the  $H^1$ -formulation continues to converge, while the slope of the  $H(\text{curl})$ -formulation



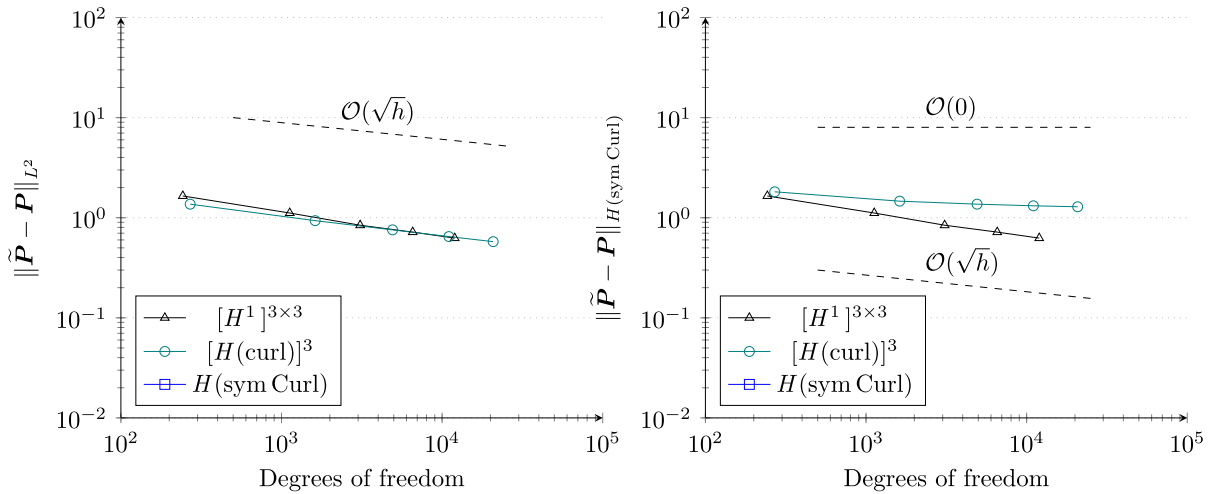


**Fig. 14** Convergence rates for the discontinuous identity benchmark

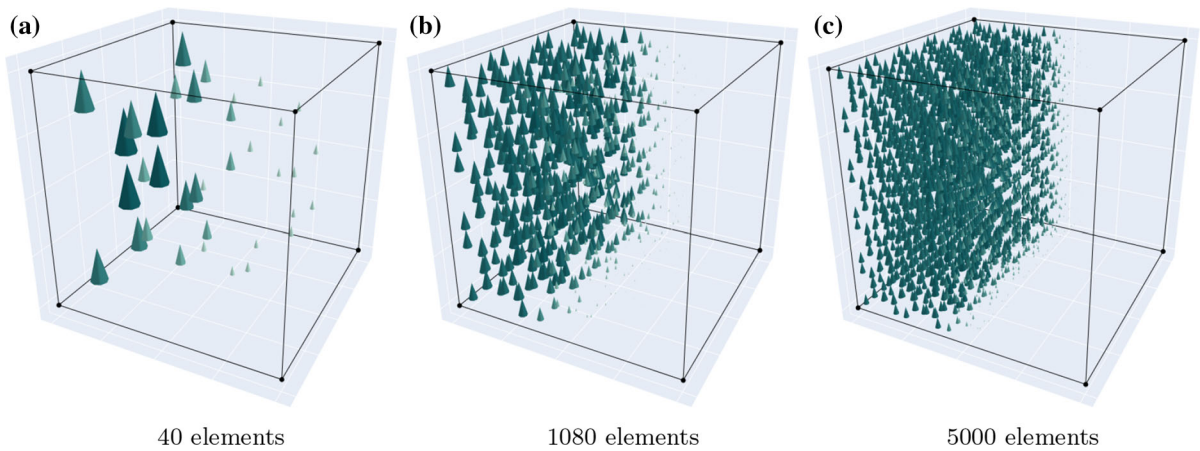


**Fig. 15** Discontinuous identity field for various discretizations of the  $H^1$ -element displaying the last row of  $\mathbf{P}$

quickly tends to zero. The errors in the solution are clearly visible in the form of noise in Figs. 16,15, whereas Fig. 17 depicts the discontinuous field as captured by the  $H(\text{sym Curl})$  formulation.

### 6 Conclusions and outlook

The relaxed micromorphic model with a symmetric micro-dislocation  $\text{sym Curl } \mathbf{P}$  as curvature measure further reduces the continuity requirements of the microdistortion field. As derived by the kernel of the trace and demonstrated by our examples, discontinuous spherical tensors can be captured by the  $H(\text{sym Curl})$ -space, as opposed to the  $[H^1]^{3 \times 3}$  and  $[H(\text{curl})]^3$  spaces. In addition, the tests show the corresponding finite element converges optimally for discontinuous spherical fields in  $H(\text{sym Curl})$ , whereas the Lagrangian and Nédélec elements exhibit sub-optimal square root convergence. Further, the convergence slope of the Nédélec-element rapidly flattens in the  $H(\text{sym Curl})$ -norm for discontinuous spherical fields.

These findings serve as a basis for understanding the behaviour of  $H(\text{sym Curl})$ -elements in implementations of the relaxed micromorphic continuum or in computations of the biharmonic equation [27]. The relaxed micromorphic complex is needed for future works, where mixed formulations of the relaxed micromorphic model with

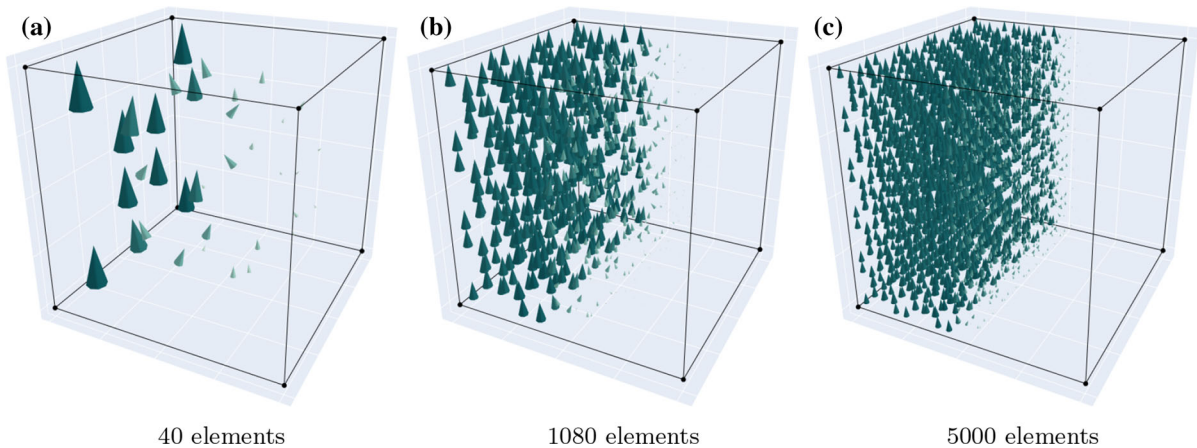


**Fig. 16** Discontinuous identity field for various discretizations of the  $H(\text{curl})$ -element displaying the last row of  $\mathbf{P}$

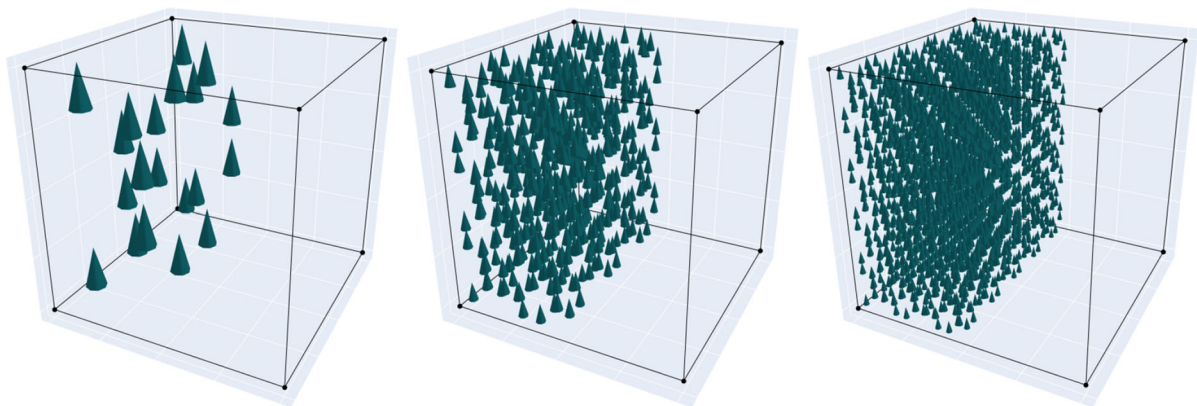


**Fig. 17** Discontinuous identity field for various discretizations of the  $H(\text{sym Curl})$ -element displaying the last row of  $\mathbf{P}$

$H(\text{sym Curl})$ - and  $H(\text{div Div})$ -conforming elements are employed to stabilize evaluation with  $L_c \rightarrow \infty$ . The latter requires the introduction of the  $H(\text{div Div})$ - or optimally  $H(\text{div Div}) \cap \text{Sym}(3)$ -conforming finite elements.

**Acknowledgements** We thank Oliver Sander (TU Dresden) for constructive discussions during drafting this manuscript. Patrizio Neff acknowledges support in the framework of the DFG-Priority Programme 2256 “Variational Methods for Predicting Complex Phenomena in Engineering Structures and Materials”, Neff 902/10-1, Project-No. 440935806.

**Funding** Open Access funding enabled and organized by Projekt DEAL.

**Open Access** This article is licensed under a Creative Commons Attribution 4.0 International License, which permits use, sharing, adaptation, distribution and reproduction in any medium or format, as long as you give appropriate credit to the original author(s) and the source, provide a link to the Creative Commons licence, and indicate if changes were made. The images or other third party material in this article are included in the article’s Creative Commons licence, unless indicated otherwise in a credit line to the material. If material is not included in the article’s Creative Commons licence and your intended use is not permitted by statutory regulation or exceeds the permitted use, you will need to obtain permission directly from the copyright holder. To view a copy of this licence, visit <http://creativecommons.org/licenses/by/4.0/>.

### A Some mathematical identities

#### A.1 The range of sym Curl

In index-notation one finds  $\text{Curl } \mathbf{P} = -P_{ij,k} \varepsilon_{jkl} \mathbf{e}_i \otimes \mathbf{e}_l$  and as such

$$\text{sym Curl } \mathbf{P} = -\frac{1}{2}(P_{ij,k} \varepsilon_{jkl} \mathbf{e}_i \otimes \mathbf{e}_l + P_{ij,k} \varepsilon_{jkl} \mathbf{e}_l \otimes \mathbf{e}_i). \tag{A.1}$$

Eliminating the constant and applying the Div operator yields

$$-2 \text{Div sym Curl } \mathbf{P} = (P_{ij,kr} \varepsilon_{jkr} \mathbf{e}_i + P_{ij,ki} \varepsilon_{jkl} \mathbf{e}_l) = P_{ij,ki} \varepsilon_{jkl} \mathbf{e}_l, \tag{A.2}$$

since the double contraction between the symmetric and anti-symmetric tensors  $P_{ij,kr} \varepsilon_{jkr}$  is zero. The next divergence operator kills the remaining term

$$-2 \text{div Div sym Curl } \mathbf{P} = P_{ij,kil} \varepsilon_{jkl} = P_{ij,ikl} \varepsilon_{jkl} = 0, \tag{A.3}$$

where the change in the order of the partial derivatives is due to Schwarz’s theorem. Therefore, there holds

$$\text{div Div sym Curl } \mathbf{P} = \frac{1}{2} \text{div Div Curl } \mathbf{P} + \frac{1}{2} \text{div Div}(\text{Curl } \mathbf{P})^T = \frac{1}{2} \text{div Div}(\text{Curl } \mathbf{P})^T = 0, \tag{A.4}$$

and

$$\text{range}(\text{sym Curl}) \subset \ker(\text{div Div}). \tag{A.5}$$

#### A.2 The kernel of sym Curl

The identity  $\ker(\text{Curl}) = \text{range}(\mathbf{D})$  is derived directly by the row-wise application of  $\ker(\text{curl}) = \text{range}(\nabla)$ . For the remaining part we consider  $\ker(\text{sym}) = \mathfrak{so}(3)$  and as such

$$\text{Curl } \mathbf{P} = \mathbf{A}, \quad \mathbf{A} \in \mathfrak{so}(3). \tag{A.6}$$

Further, we can always write  $\mathbf{A} = \text{Anti}(\mathbf{a})$  for some  $\mathbf{a} \in \mathbb{R}^3$  and consequently

$$\text{Curl } \mathbf{P} = \text{Anti}(\mathbf{a}). \tag{A.7}$$

Applying the divergence operator on both sides yields

$$\text{Div Anti}(\mathbf{a}) = \text{Anti}(\mathbf{a})_{,i} \mathbf{e}_i = \mathbf{a}_{,i} \times \mathbf{e}_i = -\text{curl } \mathbf{a} = 0, \tag{A.8}$$

since  $\text{Div Curl } \mathbf{P} = 0$ . The latter is equivalent to  $\mathbf{a} = \nabla \lambda$  for some scalar field  $\lambda : \Omega \mapsto \mathbb{R}$  on the contractible domain  $\Omega$ . Now observe that  $\text{Curl}(\lambda \mathbb{1}) = -\text{Anti}(\nabla \lambda)$  and thus  $\mathbf{P} = \lambda \mathbb{1}$  satisfies Eq. (A.7). Clearly, any other field  $\mathbf{T} = \text{Curl } \mathbf{P}$  where  $\mathbf{T} \notin \mathfrak{so}(3)$  is not in  $\ker(\text{sym Curl})$  simply because  $\mathbf{T}$  is not purely anti-symmetric and consequently, not in  $\ker(\text{sym})$ . The remaining part of the kernel is given by gradient fields, finally yielding

$$\ker(\text{sym Curl}) = \text{range}(\mathbf{D}) \cup \mathbb{R} \cdot \mathbb{1}. \tag{A.9}$$

## References

1. Mindlin RD, Eshel NN (1968) On first strain-gradient theories in linear elasticity. *Int J Solids Struct* 4(1):109–124
2. Münch I, Neff P, Wagner W (2011) Transversely isotropic material: nonlinear Cosserat versus classical approach. *Contin Mech Thermodyn* 23(1):27–34
3. Neff P, Jeong J, Ramézani H (2009) Subgrid interaction and micro-randomness—novel invariance requirements in infinitesimal gradient elasticity. *Int J Solids Struct* 46(25):4261–4276
4. Neff P, Ghiba ID, Madeo A, Placidi L, Rosi G (2014) A unifying perspective: the relaxed linear micromorphic continuum. *Contin Mech Thermodyn* 26(5):639–681
5. Askas H, Aifantis E (2011) Gradient elasticity in statics and dynamics: an overview of formulations, length scale identification procedures, finite element implementations and new results. *Int J Solids Struct* 48:1962–1990
6. Eringen A (1999) *Microcontinuum field theories. I. Foundations and solids*. Springer, New York
7. Mindlin R (1964) Micro-structure in linear elasticity. *Arch Ration Mech Anal* 16:51–78
8. Neff P, Eidel B, d'Agostino MV, Madeo A (2020) Identification of scale-independent material parameters in the relaxed micromorphic model through model-adapted first order homogenization. *J Elast* 139(2):269–298
9. Ebobisse F, Neff P (2010) Existence and uniqueness for rate-independent infinitesimal gradient plasticity with isotropic hardening and plastic spin. *Math Mech Solids* 15(6):691–703
10. Ebobisse F, Neff P, Aifantis EC (2018) Existence result for a dislocation based model of single crystal gradient plasticity with isotropic or linear kinematic hardening. *Quart J Mech Appl Math* 71(1):99–124
11. Ebobisse F, Neff P, Forest S (2018) Well-posedness for the microcurl model in both single and polycrystal gradient plasticity. *Int J Plast* 107:1–26
12. Ebobisse F, Hackl K, Neff P (2019) A canonical rate-independent model of geometrically linear isotropic gradient plasticity with isotropic hardening and plastic spin accounting for the burgers vector. *Contin Mech Thermodyn* 31(5):1477–1502
13. Madeo A, Neff P, Ghiba ID, Rosi G (2016) Reflection and transmission of elastic waves in non-local band-gap metamaterials: a comprehensive study via the relaxed micromorphic model. *J Mech Phys Solids* 95:441–479
14. Madeo A, Barbagallo G, Collet M, d'Agostino MV, Miniaci M, Neff P (2018) Relaxed micromorphic modeling of the interface between a homogeneous solid and a band-gap metamaterial: new perspectives towards metastructural design. *Math Mech Solids* 23(12):1485–1506. <https://doi.org/10.1177/1081286517728423>
15. Rizzi G, Hütter G, Khan H, Ghiba ID, Madeo A, Neff P (2022) Analytical solution of the cylindrical torsion problem for the relaxed micromorphic continuum and other generalized continua (including full derivations). *Math Mech Solids* 27(3): 507–553. <https://doi.org/10.1177/108128652111023530>
16. Rizzi G, Hütter G, Madeo A, Neff P (2021) Analytical solutions of the cylindrical bending problem for the relaxed micromorphic continuum and other generalized continua. *Contin Mech Thermodyn* 33(4):1505–1539
17. Rizzi G, Hütter G, Madeo A, Neff P (2021) Analytical solutions of the simple shear problem for micromorphic models and other generalized continua. *Arch Appl Mech* 91:2237–2254
18. Sky A, Neunteufel M, Münch I, Schöberl J, Neff P (2021) A hybrid  $H^1 \times H(\text{curl})$  finite element formulation for a relaxed micromorphic continuum model of antiplane shear. *Comput Mech* 68(1):1–24
19. Schröder J, Sarhil M, Scheunemann L, Neff P (2021) Lagrange and  $H(\text{curl}, \mathcal{B})$  based finite element formulations for the relaxed micromorphic model. *Comput Mech*
20. Sky A, Neunteufel M, Muench I, Schöberl J, Neff P (2022) Primal and mixed finite element formulations for the relaxed micromorphic model. *Comput Methods Appl Mech Eng* 399(115):298
21. Bauer S, Neff P, Pauly D, Starke G (2014) New Poincaré-type inequalities. *CR Math* 352(2):163–166
22. Bauer S, Neff P, Pauly D, Starke G (2016) Dev-Div- and DevSym-DevCurl-inequalities for incompatible square tensor fields with mixed boundary conditions. *ESAIM* 22(1):112–133
23. Lewintan P, Neff P (2021)  $L^p$ -trace-free generalized Korn inequalities for incompatible tensor fields in three space dimensions. *Proc R Soc Edinb* 1–32
24. Lewintan P, Neff P (2021)  $L^p$ -versions of generalized Korn inequalities for incompatible tensor fields in arbitrary dimensions with  $p$ -integrable exterior derivative. *CR Math* 359(6):749–755
25. Lewintan P, Neff P (2021) Nečas-Lions lemma revisited: An  $L^p$ -version of the generalized Korn inequality for incompatible tensor fields. *Math Methods Appl Sci* 44(14):11392–11403
26. Lewintan P, Müller S, Neff P (2021) Korn inequalities for incompatible tensor fields in three space dimensions with conformally invariant dislocation energy. *Calc Var Partial Differ Equ* 60(4):150
27. Pauly D, Zulehner W (2020) The divDiv-complex and applications to biharmonic equations. *Appl Anal* 99(9):1579–1630
28. Nedelec JC (1980) Mixed finite elements in  $\mathbb{R}^3$ . *Numer Math* 35(3):315–341
29. Nédélec JC (1986) A new family of mixed finite elements in  $\mathbb{R}^3$ . *Numer Math* 50(1):57–81
30. Schöberl J, Zaglmayr S (2005) High order Nédélec elements with local complete sequence properties. *COMPEL* 24(2):374–384
31. Zaglmayr S (2006) High order finite element methods for electromagnetic field computation. PhD thesis, Johannes Kepler Universität Linz, <https://www.numerik.math.tugraz.at/~zaglmayr/pub/szthesis.pdf>
32. Sander O (2021) Conforming finite elements for  $H(\text{sym Curl})$  and  $H(\text{dev sym Curl})$ . arXiv abs/2104.12825, <https://arxiv.org/abs/2104.12825>, 2104.12825

33. Ghiba ID, Neff P, Madeo A, Placidi L, Rosi G (2015) The relaxed linear micromorphic continuum: existence, uniqueness and continuous dependence in dynamics. *Math Mech Solids* 20(10):1171–1197. <https://doi.org/10.1177/1081286513516972>
34. Ghiba ID, Neff P, Owczarek S (2021) Existence results for non-homogeneous boundary conditions in the relaxed micromorphic model. *Math Methods Appl Sci* 44(2):2040–2049
35. Neff P, Ghiba ID, Lazar M, Madeo A (2015) The relaxed linear micromorphic continuum: well-posedness of the static problem and relations to the gauge theory of dislocations. *Q J Mech Appl Math* 68(1):53–84
36. d'Agostino MV, Rizzi G, Khan H, Lewintan P, Madeo A, Neff P (2021) The consistent coupling boundary condition for the classical micromorphic model: existence, uniqueness and interpretation of parameters. [arxiv2112.12050](https://arxiv.org/abs/2112.12050)
37. Demkowicz L, Monk P, Vardapetyan L, Rachowicz W (2000) De Rham diagram for hp-finite element spaces. *Comput Math Appl* 39(7):29–38
38. Arnold DN, Hu K (2021) Complexes from complexes. *Found Comput Math* 21(6):1739–1774. <https://doi.org/10.1007/s10208-021-09498-9>
39. Hu J, Liang Y, Ma R (2021) Conforming finite element DIVDIV complexes and the application for the linearized Einstein-Bianchi system. *ResearchGate* [https://www.researchgate.net/publication/349704589\\_Conforming\\_finite\\_element\\_DIVDIV\\_complexes\\_and\\_the\\_application\\_for\\_the\\_linearized\\_Einstein-Bianchi\\_system](https://www.researchgate.net/publication/349704589_Conforming_finite_element_DIVDIV_complexes_and_the_application_for_the_linearized_Einstein-Bianchi_system)
40. Neff P, Pauly D, Witsch KJ (2012) Maxwell meets Korn: a new coercive inequality for tensor fields with square-integrable exterior derivative. *Math Methods Appl Sci* 35(1):65–71
41. Neff P, Pauly D, Witsch KJ (2015) Poincaré meets Korn via Maxwell: extending Korn's first inequality to incompatible tensor fields. *J Differ Equ* 258(4):1267–1302. <https://doi.org/10.1016/j.jde.2014.10.019>

**Publisher's Note** Springer Nature remains neutral with regard to jurisdictional claims in published maps and institutional affiliations.